JOURNAL OF MATERIALS SCIENCE 29 (1994) 1507–1513

Sintering of $(Ca_{1-x}, Mg_x)Zr_4(PO_4)_6$ ceramics

DEAN-MO LIU
Materials Research Laboratories, Industrial Technology Research Institute, Hsingchu, Chutung, 31015, Taiwan

Densification and grain growth of $(Ca_{1-x}, Mg_x)Zr_4(PO_4)_6$ (CMZP; where $x=0.0$, 0.1, and 0.4) ceramics at the intermediate stage of sintering have been investigated. A lattice-diffusion model proposed by Coble with tetrakaidecahedron as a grain shape was employed and appears to be applicable to the sintering of CMZP. The apparent diffusion coefficient of the CMZP ceramics for $x=0.0$ is lower by approximately three and one orders of magnitude than for $x=0.1$ and $x=0.4$, respectively. The grain growth in CMZP at the intermediate stage of sintering follows a third-power kinetics, i.e. $n=3$. A modified expression using the lattice-diffusion model associated with grain-growth kinetics has been derived which makes the microstructures of CMZP controllable.

1. Introduction

$(Ca_{1-x}, Mg_x)Zr_4(PO_4)_6$ (CMZP) ceramics with $x = 0.0$, 0.1, and 0.4, were synthesized by incorporating magnesium into the $CaZr_4(PO_4)_6$. The CMZP ceramics possess a framework structure which resembles that of the well-known [NZP] which consists of PO_4 tetrahedra and ZrO_6 octahedra linked by corners, and belongs to $R\bar{3}c$ space group [1–3].

In reviewing the sintering kinetics of ceramic materials, most of the investigations have been focused on materials such as Al_2O_3 [4], ZnO [5], MgO [6, 7], and BeO [8, 9]. However, available reports for simultaneous measurements of grain growth and densification are rare and those which have appeared in the literature are limited to materials such as Al_2O_3 [10], ZnO [5], and BeO [8].

Upon determining the diffusion mechanisms that dominate the sintering behaviour, the grain-size factor usually plays a key role in estimating the resulting kinetic parameters [11]. In the present study, a simultaneous measurement of grain growth and densification during sintering was performed in CMZP in an attempt to understand which possible diffusion mechanism is predominant and to study the coarsening–densification competition. A lattice-diffusion model which was proposed by Gupta and Coble [5, 11] for densification at the intermediate stage of sintering was employed because of its wide applicability to a number of materials [8, 10, 11]. The model which is postulated for grains with cylindrical pores on the edges of a truncated octahedron is given as [5, 10]

$$\left\{P^{3/2}\left[1 + \ln\left(\frac{4P}{3.33}\right)^{-3/2}\right]\right\}_1^2 = -1190\frac{D_1\gamma\delta}{G^3kT}t\Bigg]_1^2 \quad (1)$$

where P is the volume fraction of porosity, D_1 the apparent lattice diffusion coefficient, γ the surface energy, δ the lattice volume, G the average grain size, k the Boltzmann constant, T the absolute temperature, and t is the firing period.

The apparent diffusion coefficient, D_1, in Equation 1 was usually obtained by averaging several points from which were determined, by extrapolation, the appropriate density and grain-size curves; equal slopes and constant grain size were usually assumed. However, Clare [8] proposed a simple mathematical treatment using Coble's model and successfully obtained an expression that renders the microstructures of beryllium oxide controllable. In this work, a modified model based on Equation 1 and Clare's treatment using f as a function of porosity is performed.

The grain-growth kinetics is estimated by the purely well-known empirical equation

$$G^3 - G_0^3 = Kt \quad (2)$$

where G_0 is the average grain size at $t = 0$ and K the temperature-dependent rate constant. The growth-rate constant, K, and the apparent diffusion coefficient, D_1, are both temperature dependent

$$K = K_0\exp(-E_1/RT) \quad (3)$$

$$D_1 = D_0\exp(-E_2/RT) \quad (4)$$

where K_0 and D_0 are temperature-independent factors, E_1 represents the activation energy for grain-boundary migration, and E_2, the activation energy for self-diffusion.

2. Experimental procedure

2.1. CMZP powder preparation

Single-phase CMZP powders were synthesized by a sol–gel process; the reagent-grade $Ca(NO_3)_2\cdot 4H_2O$ (98.5%, Hanawa Inc.), $Mg(NO_3)_2\cdot 6H_2O$ (98.5%, Hanawa Inc.), $ZrO(NO_3)_2\cdot xH_2O$ (99.0%, Hanawa Inc.), and H_3PO_4 (85%, Merck) which were used as starting materials, were prepared to form 1.0 M aqueous solutions. The zirconium nitrate and a nitrate

0022–2461

solution containing calcium and magnesium ions with the desired molar ratios were mixed first. The phosphate solution was adjusted to pH 9 by ammonium water prior to adding to the nitrate solution, which was stirred vigorously. The pH value of the solution was kept at 9–10 by adding ammonium hydroxide until the solution became a gel. The gel was dried at 40 °C for 24 h, and then calcined at 900–1000 °C for 24 h to drive off the nitrates and resulted in fine single-phase powders having an average particle size of 45–50 nm.

2.2. Sintering and density measurement

The CMZP powders were compacted in a stainless-steel die under a hydraulic pressure of 30 MPa. The samples were approximately 0.4 in diameter and 0.2 in thick. The die-pressed pellets were gassed by placing it in a plastic bag, then by cold-isostatically pressing at 200 MPa for 5 min. The green density of the specimens was about 50%–52% theoretical densities, which are 3.20, 3.194 and 3.174 g cm^{-3} for $x = 0.0$, 0.1, and 0.4, respectively. The pellets were then sintered at 1050–1300 °C at a heating rate of 10 °C min^{-1} for various periods, then cooled at a rate of 30 °C min^{-1}. The densities of the as-sintered pellets were determined using Archimede's method with water as an immersing medium.

2.3. Grain-size measurement

The specimens used for grain-growth observation were prepared from those used for density measurement. Observations of grain growth were made on polished specimens prepared by wet grinding with 600-grit silicon carbide paper followed by polishing on a cloth-covered lap with 1 μm α-alumina, then etching in 1.5 N hot HCl solution. The average grain size, G, of the sintered CMZP was determined by examining the polished surface using scanning electron microscopy (Cambridge Instruments, S-360 system) using a linear-intercept technique [12], and approximately 120 grains were counted for each sample.

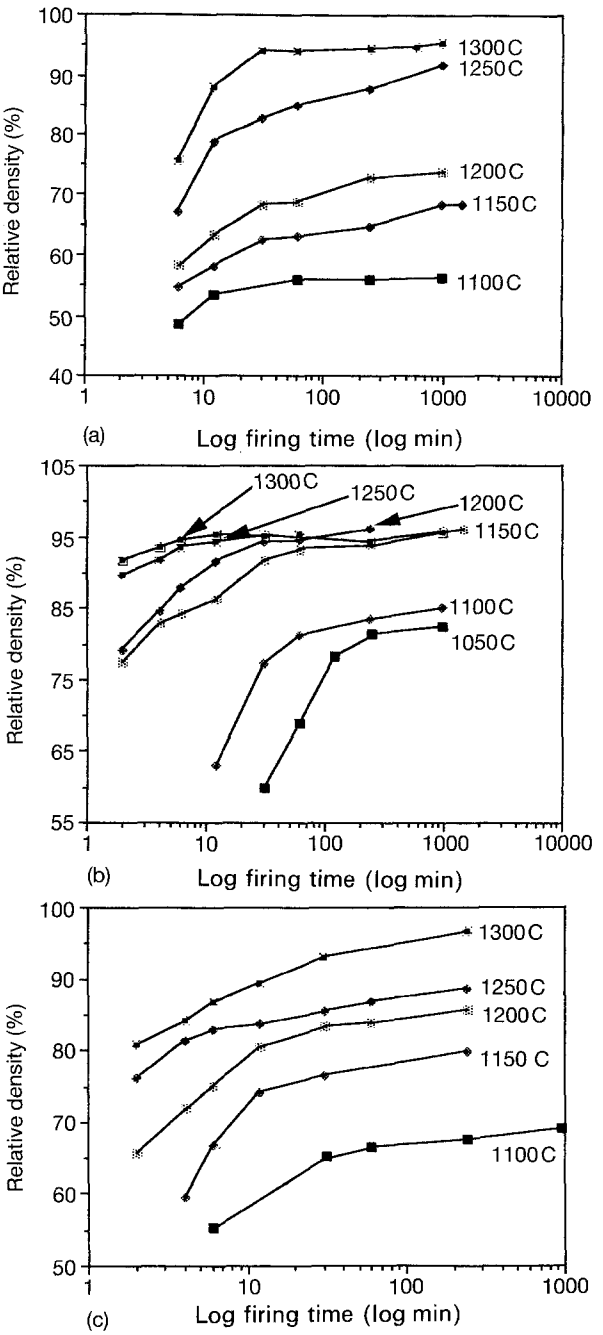

Figure 1 Isothermal densification of CMZP versus firing time at various temperatures. (a) $x = 0.0$, (b) $x = 0.1$, (c) $x = 0.4$.

3. Results

3.1. Densification

Isothermal densification versus log time is depicted in Fig. 1a–c for compositions of 0.0, 0.1, and 0.4, respectively. These plots show an initial increase in densification with time at temperatures of 1050–1300 °C, then followed by little or no increase for extended times. In fact, the relative densities of the CMZP tend to reach a limiting density at each temperature, and above 95% theoretical density, can be reached immediately after a short period of firing above 1250 °C.

3.2. Grain growth

Fig. 2a–c illustrate the results of log grain size versus log firing time for CMZP with compositions of $x = 0.0$, 0.1, and 0.4, respectively, from 1050–1300 °C. The relations show a slight non-linearity with a few scattered points, which is probably due to the effect of pores [13, 14], or a possible temperature shift. However, the most reliable data are best represented by applying a purely empirical third-power kinetics [10] with the consideration of initial grain size, G_0, as in Fig. 3a–c. The well-fitted linear results sufficiently reveal that the grain growth is beyond the theoretical description in which grain growth follows the square root of time, i.e. $n = 2$, and this difference is caused by the presence of secondary phase, e.g. pores [13].

4. Discussion

4.1. Kinetics of densification

As sintering proceeds, the relative densities of CMZP increase and reach a limiting point where no further increase in density has occurred. The initial portion of the curves is associated with the intermediate stage of

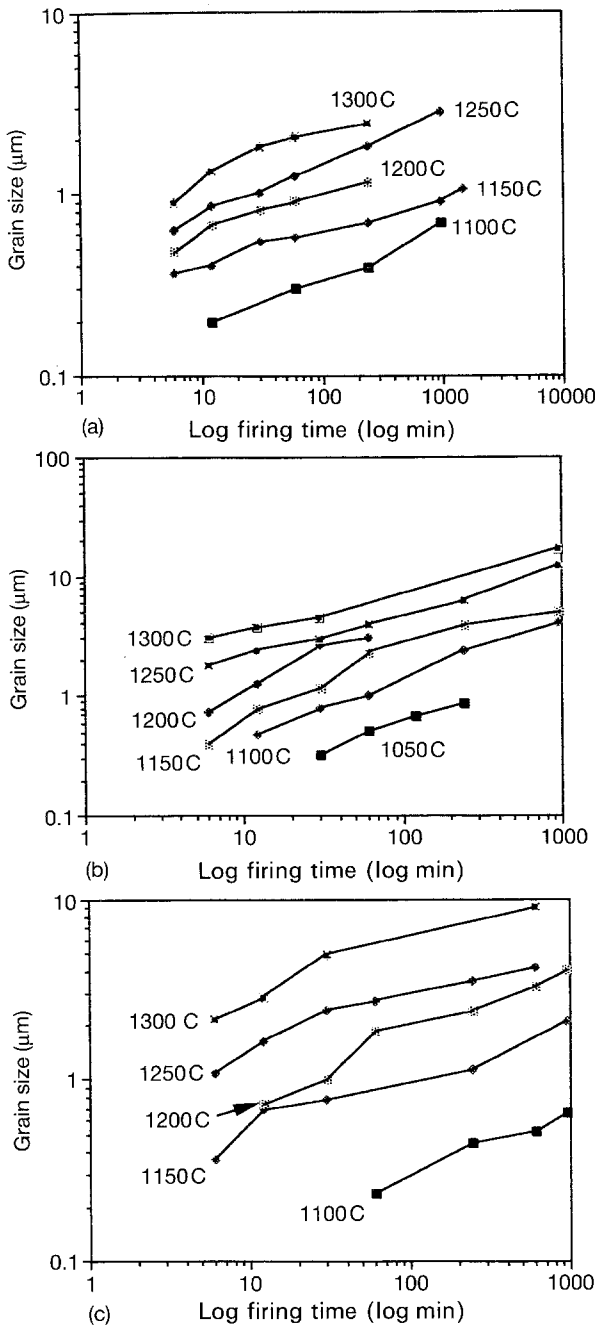

Figure 2 Isothermal grain growth versus firing time at various temperatures. (a) $x = 0.0$, (b) $x = 0.1$, (c) $x = 0.4$.

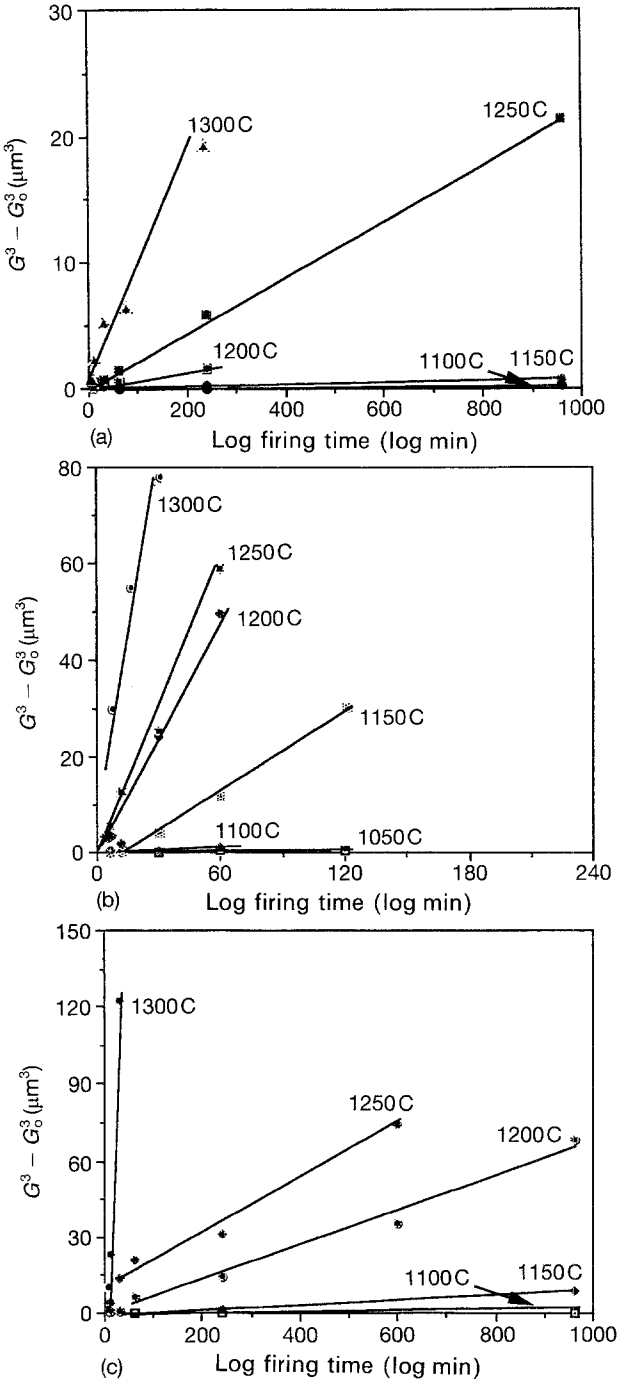

Figure 3 Grain size with third-power kinetics versus time. (a) $x = 0.0$, (b) $x = 0.1$, (c) $x = 0.4$.

sintering and the regions, usually at a density greater than 95% TD, where little or no change in density represents the final stage of sintering. The sintering kinetics of the CMZP was first approached by a lattice-diffusion model proposed by Coble [5]. The apparent diffusion coefficients of CMZP can be estimated by letting

$$f = \left\{P^{3/2}\left[1 + \ln\left(\frac{4P}{3.33}\right)^{-3/2}\right]\right\}_1^2 \qquad (5)$$

Fig. 4 is a plot of f versus porosity, p, where f is proportional to porosity, p, and shows a nearly linear relationship in porosities of 5%–40%. A small interval of porosity change can be represented as a small change in f. Thus for a differential change in f in an infinitesimal period of firing, Equation 1 can be rewritten in association with Equation 2 and G_0 is assumed to be negligible, thus

$$\mathrm{d}f\int_{f_0}^{f} = -1190\frac{D_1\gamma M}{K\rho RTt}\mathrm{d}t\int_{t=0}^{t=t} \qquad (6)$$

After integration, Equation 6 becomes

$$f = f_0 - 1190\frac{D_1\gamma M}{K\rho RT}\ln t \qquad (7)$$

where f_0 represents f at the corresponding green density and the apparent diffusion coefficient, D_1, can be determined by plotting f in terms of natural logarithmic t by assuming the densification mechanism is the same for whole intermediate stage of sintering. Fig. 5a–c are plots for $x = 0.0$, 0.1, and 0.4, respectively, where D_1 can be calculated from the slopes at each temperature under assumption of constant surface energy, γ, to be 1000 erg cm^{-2} in the study temperatures.

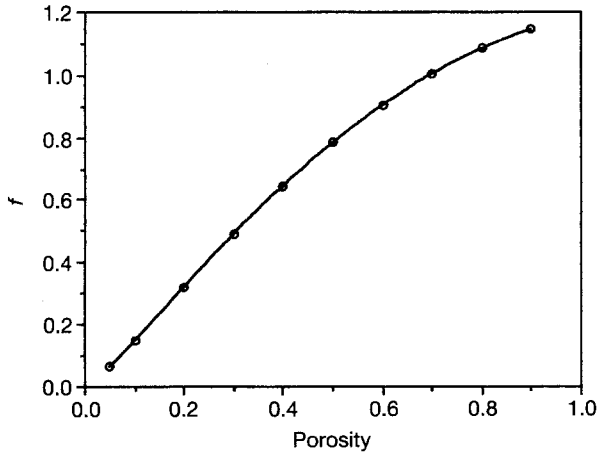

Figure 4 Calculation of f as a function of porosity, p.

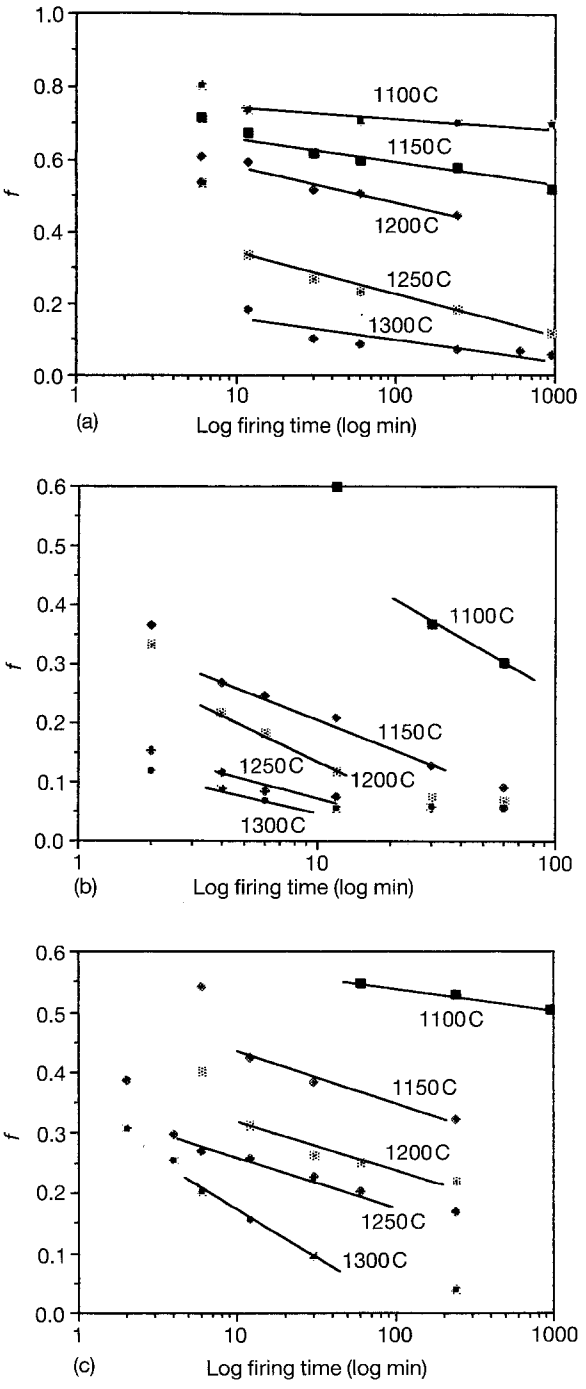

Figure 5 Values of f with respect to logarithmic firing time. (a) $x = 0.0$, (b) $x = 0.1$, (c) $x = 0.4$.

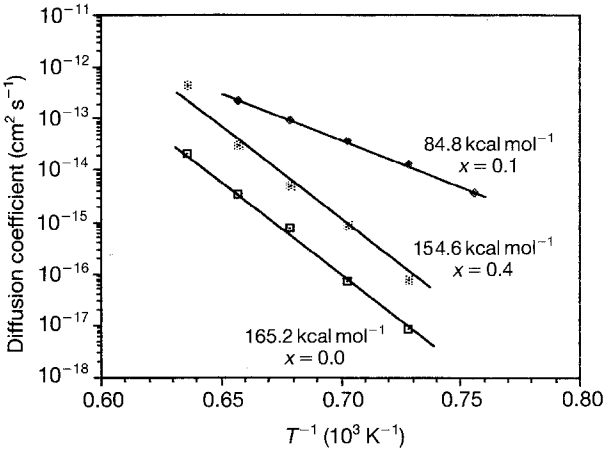

Figure 6 Apparent diffusion coefficients of CMZP in terms of reciprocal absolute temperature.

Fig. 6 shows the calculated apparent diffusion coefficients, in an Arrhenius sense, between 1050 and 1300 °C. The resulting expressions for the diffusion coefficients for compositions 0.0, 0.1, and 0.4 are

$$D_{0.0} = 1.97 \times 10^9 \exp(-165\,200/RT \text{ cal})\ \text{cm}^2\,\text{s}^{-1} \quad (8)$$

$$D_{0.1} = 0.32 \exp(-84\,400/RT \text{ cal})\ \text{cm}^2\,\text{s}^{-1} \quad (9)$$

$$D_{0.4} = 2.4 \times 10^8 \exp(-154\,600/RT \text{ cal})\ \text{cm}^2\,\text{s}^{-1} \quad (10)$$

respectively. The activation energies for densification of CMZP demonstrate a strong dependence on magnesium content; where the coefficients for $x = 0.1$ and 0.4 (i.e. $D_{0.1}$ and $D_{0.4}$, respectively) are higher by approximately three and one orders of magnitude, respectively, than for $x = 0.0$. The lower activation energy for material diffusion indicates a higher rate of densification and is associated with the conclusion that magnesium addition increases the rate of lattice diffusion, but tends to retard the diffusion rate, while further increase of magnesium, which may result from the decrease of lattice volume [17], restricts the rate of matter diffusion.

4.2. Kinetics of grain growth

The grain growth during sintering is illustrated in a plot of time versus third-power of grain size in Fig. 3, in which $n = 3$ gives a best-fit result. The temperature dependence for the grain growth at the intermediate stage of sintering can be obtained using the slopes in Fig. 3 and Equation 3 through an Arrhenius plot, as illustrated in Fig. 7. The resulting values are 120.5, 104.8, and 133.1 kcal mol^{-1} for 0.0, 0.1, and 0.4, respectively, and can be further expressed as

$$K_{0.0} = 63.1 \exp(-120\,400/RT \text{ cal})\ \text{cm}^3\,\text{s}^{-1} \quad (11)$$

$$K_{0.1} = 27.5 \exp(-104\,800/RT \text{ cal})\ \text{cm}^3\,\text{s}^{-1} \quad (12)$$

and

$$K_{0.4} = 1.9 \times 10^4 \exp(-133\,100/RT \text{ cal})\ \text{cm}^3\,\text{s}^{-1} \quad (13)$$

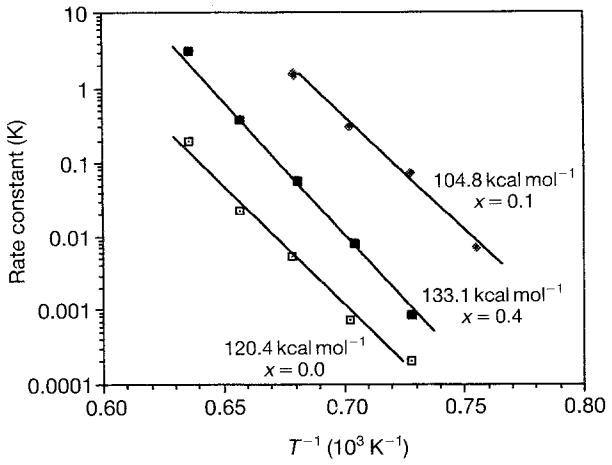

Figure 7 Rate constant of grain growth in terms of reciprocal absolute temperature.

In fact, it is difficult to determine which species is predominant owing to the complexity of constituting components, i.e. calcium, magnesium, zirconium, phosphorus and oxygen. However, a coexisting diffusion mechanism possibly takes place during sintering such as those reported in Al_2O_3 [14] and $Ca_{0.16}Zr_{0.84}O_{1.84}$ [15, 16]. The difference in activation energy, i.e. from 120.4 kcal mol^{-1} for $x = 0.0$ to 104.8 kcal mol^{-1} for $x = 0.1$ for grain-boundary migration due to different magnesium contents, may result from the faster-diffusing species, e.g. magnesium having a smaller ionic radius that is present. However, the energy considerably increases after further increase of magnesium, i.e. 133.1 kcal mol^{-1} for $x = 0.4$. Van Aken [17] has reported that the lattice volume of CMZP decreased while sufficient amounts of calcium were being replaced by magnesium. Therefore, it is normal to realize that the increased activation energy in higher magnesium-content CMZP is a result of decreased lattice volume that usually limits the diffusion path and results in retarding the rate of material diffusion. Furthermore, the similar trend in energy variation for grain growth, as well as for densification due to magnesium content, strongly suggests the contribution of lattice diffusion, although the diffusion mechanisms for grain growth and for densification are essentially different.

Additionally, grain-boundary diffusion may also play an important role in grain growth during sintering because the activation energy for lattice diffusion is higher than that for grain-boundary diffusion [18]. Hence, the energy difference in grain growth and lattice-diffusion-controlled densification may be evidence. Therefore, although not conclusive, the grain growth in CMZP during sintering is strongly suggested to be dominated by a multimodal diffusion mechanism, and which of the mechanisms is important may depend on microstructure evolution [19].

On comparing with the grain growth in the final stage of sintering [20], the activation energy is considerably lower than that in the present results once magnesium was introduced. This difference is primarily due to the presence of pores that inhibit grain-boundary migration and lead to an increased activation energy.

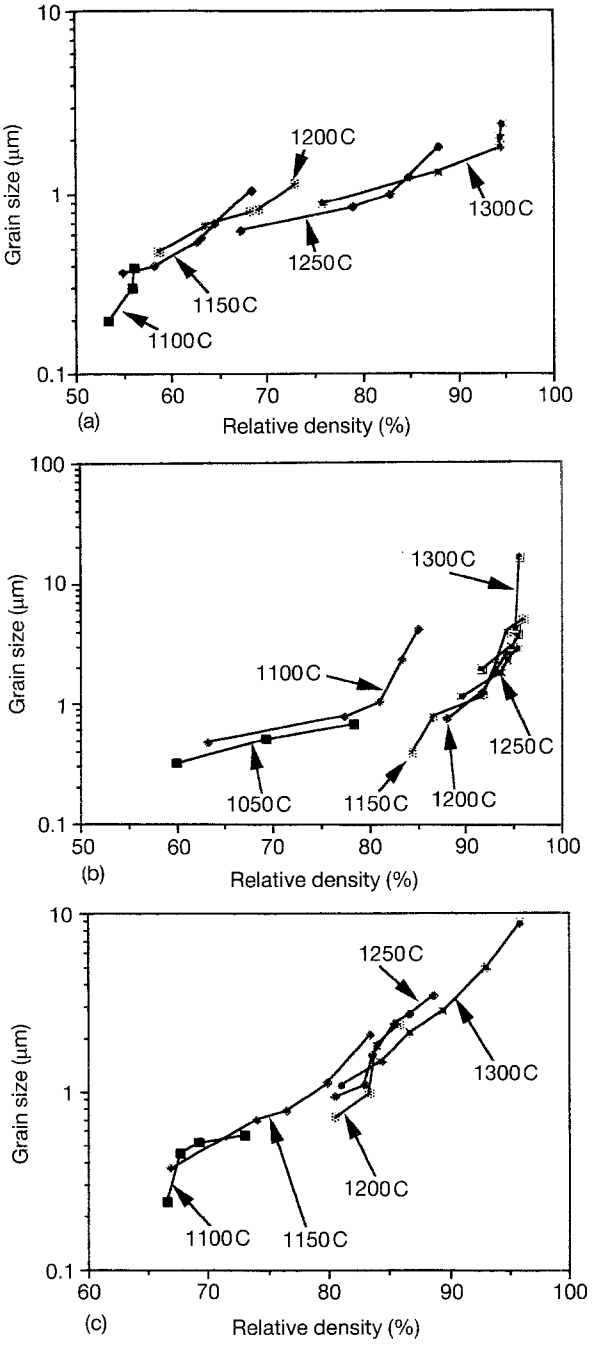

Figure 8 Variations of grain size with change of relative density. (a) $x = 0.0$, (b) $x = 0.1$, (c) $x = 0.4$.

4.3. Grain size and relative density

Fig. 8a–c are plots of the logarithmic grain size versus relative density of CMZP at various sintering temperatures. As shown, except for $x = 0.1$ in which the grain grows rapidly only at higher relative densities, grain growth is in proportion to the increase of relative density for $x = 0.0$ and 0.4. Grain growth in CMZP, however, appears to be temperature dependent and is suggested to have an effect on the kinetics of sintering [11, 19].

When considering the competition between grain growth (i.e. coarsening) and densification in CMZP during sintering, especially for those exhibiting a higher activation energy for densification than for grain growth, an attempt to describe the qualitative relation between this competition has been rationalized using the ratio of the diffusion coefficient, D_l,

and rate constant, K, from Equations 3 and 4, thus

$$\frac{D_1}{K} = \frac{D_0}{K_0}\exp\left(\frac{E_1 - E_2}{RT}\right) \quad (14)$$

where the values of (D_0/K_0) and $(E_1 - E_2)$ are listed in Table I. Fig. 9 shows a plot of D_1/K versus T, indicating that higher-temperature sintering is preferred for $x = 0.0$ and 0.4, but lower temperature is favourable for 0.1 because the rate of grain growth for $x = 0.1$ is largely enhanced at elevated temperatures.

It is important to obtain a dense or porosity-controllable ceramic compact with grain size as small as possible, especially for those materials having thermal expansion anisotropy such as CMZP [18, 21]. Clare [8] has successfully used sintering kinetics data with a theoretically derived equation to obtain a beryllium oxide with controllable porosity and minimum grain size at a pre-determined sintering temperature. In this study, essentially the same expression derived in a fashion similar to that reported by Clare has been used, but instead the porosity, p, is replaced by f (which is defined in Equation 5). Thus

$$f = f_0 - \frac{B}{T}\frac{E_1}{(E_2 - E_1 - RT)}\exp\left(\frac{E_1 - E_2}{RT}\right) \quad (15)$$

where

$$B = 1190\frac{D_0\gamma M}{K_0\rho R} \quad (16)$$

is a constant, as listed in Table I. After rearrangement, Equation 15 becomes

$$(E_2 - E_1 - RT)\exp\left(\frac{E_2 - E_1}{RT}\right) = \frac{E_1}{f_0 - f}\frac{B}{T} \quad (17)$$

Equation 17 is only theoretically valid for conditions of $(E_2 - E_1 - RT)$ greater than zero, i.e. the activation energy for densification is sufficiently higher than that for grain growth. Thus for a given porosity, i.e. f is fixed, T in the right-hand term of Equation 17 times the left-hand term of the equation, results in a constant value (i.e. $E_1B/f_0 - f$), because E_1, f_0, and B are constants. By substituting the values in Table I into Equation 17 and plotting T in terms of $(E_2 - E_1 - RT)\exp(E_2 - E_1/RT)$, Fig. 10a and b, with open circles for $x = 0.0$ and 0.4, respectively. For CMZP at 95% theoretical density, the optimum temperature for $x = 0.0$ is about 1300–1350 °C and for $x = 0.4$, 1350–1400 °C, to have a minimum grain size. This appears to be very consistent with the results of Fig. 9 that higher temperatures are favourable at $x = 0.0$ and 0.4 for densification.

Additionally, the sintering period for CMZP to densify to any given density at a specific temperature can thus be given by combining Equations 7, 14, and 16. After rearrangement

$$\ln t = \frac{1}{f_0 - f}\frac{T}{B}\exp\left(\frac{E_1 - E_2}{RT}\right) \quad (18)$$

For 95% theoretical density, the shortest time at various temperatures for $x = 0.0$ and 0.4 is shown in Fig. 10a and b with closed circles, respectively. Table II demonstrates a list of calculated results for obtaining CMZP at 95% TD with minimum grain size at different pre-determined sintering temperatures. The experimental observations are also listed in the last column by interpolating the curves in Fig. 2a and c for comparison: the observed grain sizes are larger than the calculated values.

This occurrence of the deviation is caused by neglecting the initial grain size, G_0, at the very beginning

TABLE I Calculated results of (D_0/K_0), $(E_1 - E_2)$, and constant B

x	D_0/K_0 (cm^{-1})	$E_1 - E_2$ (cal)	B
0.0	3.1×10^7	− 44 800	5.7×10^8
0.1	0.012	+ 20 400	3.2×10^3
0.4	1.3×10^4	− 21 500	2.4×10^5

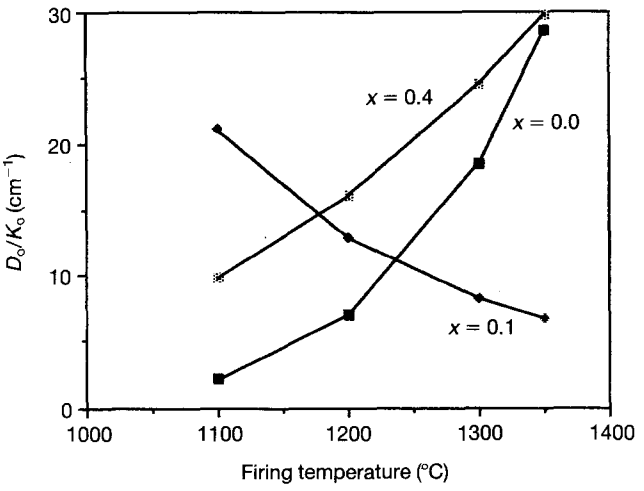

Figure 9 Ratios of densification rate and grain growth rate in terms of temperature.

TABLE II List of the calculated results for obtaining a CMZP with a minimum grain size at a preset density of 95% TD at various predetermined sintering temperatures. The experimental observations are listed in the last column for comparison

T (°C)	Calculated time (s)		Calculated grain size (μm)		Observed grain size (μm)	
	$x = 0.0$	$x = 0.4$	$x = 0.0$	$x = 0.4$	$x = 0.0$	$x = 0.4$
1300	64	5430	0.9	3.21	1.3[a]	6.3[b]
1350	72	1650	0.65	3.34		
1400	20	522	0.62	3.43		

[a] At corresponding relative density 92%.
[b] At corresponding relative density 94.7%.

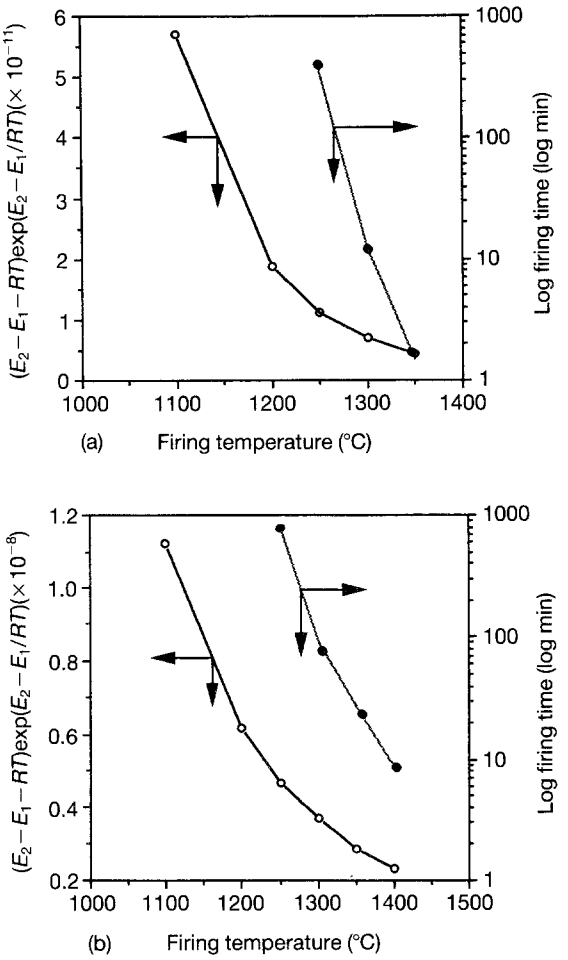

Figure 10 Calculated $(E_2 - E_1 - RT)\exp(E_2 - E_1/RT)$ with respect to temperature for CMZP at 95% theoretical density. (a) $x = 0.0$, (b) $x = 0.4$.

of the derivation, Equation 6. However, the corresponding relative densities under the same sintering conditions obtained experimentally for $x = 0.0$ and 0.4 are 92% and 94.7% (data from Fig. 1a and c), of which the latter is closer to the preset 95% than the former. In other words, the modified model gives a good prediction of the sintering of CMZP. The discrepancy in density for $x = 0.0$ suggests a tendency for discontinuous grain growth to occur during sintering.

5. Conclusion

The grain growth and densification of CMZP at the intermediate stage of sintering have been investigated at temperatures of 1050–1300 °C. The grain growth in CMZP appears to be dominated by a multimodal diffusion mechanism, i.e. lattice and grain-boundary diffusion, and follows the third-power kinetics. A lattice-diffusion model appears to be applicable to densification during sintering, from which the resulting apparent diffusion coefficient for $x = 0.0$ is lower by one to three and one orders of magnitude for $x = 0.1$ and 0.4, respectively, suggesting that the magnesium does increase the rate of densification. A model conducted by modifying Coble's diffusion expression associated with Clare's derivation is postulated, and seems to have good agreement with experimental results. In general, to obtain a dense CMZP with the smallest grain sizes, a higher heating rate to minimize the initial grain size, G_0, and sufficient magnesium content to avoid the tendency of discontinuous grain growth, are essentially required.

Acknowledgements

The author thanks Ministry of Economic Administration, Taiwan, for supporting this research.

References

1. G. E. LENAIN, H. A. McKINSTRY, J. ALAMO and D. K. AGRAWAL, *J. Mater. Sci.* **22** (1987) 17.
2. J. ALAMO and R. ROY, *ibid.* **21** (1986) 444.
3. S. Y. LIMAYE, D. K. AGRAWAL and H. A. McKINSTRY, *J. Am. Ceram. Soc.* **70** (1987) c232.
4. S. J. BENNISM and M. P. HARMER, in "Ceramic Transaction", Vol. 7, "Sintering of Advanced Ceramics", edited by C. A. Handwerker, J. E. Blendell and W. A. Kagsser (American Ceramic Society, 1990) pp. 13–49.
5. T. K. GUPTA and R. L. COBLE, *J. Am. Ceram. Soc.* **51** (1968) 521.
6. R. M. SPRIGGS, L. A. BRISSETLE and T. VASILOS, *ibid.* **47** (1964) 417.
7. *Idem, ibid.* **46** (1963) 508.
8. T. E. CLARE, *ibid.* **49** (1966) 159.
9. M. J. BAMNISTER, *J. Nucl. Mater.* **14** (1964) 315.
10. R. L. COBLE, *J. Appl. Phys.* **32** (1961) 793.
11. R. L. COBLE and T. K. GUPTA, in "Sintering and Related Phenomena", edited by G. C. Kuczynski, N. A. Hroton and C. F. Gibbon (Gordon and Breach, New York, 1967) pp. 423–41.
12. D. TURNBULL, *J. Metals 3 Trans. AIME* **191** (1951) 661.
13. W. D. KINGERY and B. FRANCOIS, *J. Am. Ceram. Soc.* **48** (1965) 546.
14. R. L. COBLE, *J. Appl. Phys.* **36** (1965) 2327.
15. T. Y. TIEN and E. C. SUBBARAO, *J. Am. Ceram. Soc.* **46** (1963) 489.
16. W. H. RHODES and R. E. CARTER, *Am. Ceram. Soc. Bull.* **41** (1962) 283.
17. S. M. VAN AKEN, MS thesis, Virginia Polytechnic Institute and State University (1990).
18. J. E. BURKE, *J. Am. Ceram. Soc.* **40** (1957) 80.
19. J. H. ROSOLOWSKI and C. GRESKOVICH, *ibid.* **58** (1975) 177.
20. D. M. LIU, *J. Mater. Sci.* **28** (1993) 6353.
21. D. M. LIU and J. J. BROWN Jr., *J. Mater. Chem. Phys.* **33** (1993) 43.

Received 23 September 1992
and accepted 27 September 1993